ELSEVIER

NeuroImage

www.elsevier.com/locate/ynimg
NeuroImage 31 (2006) 1025 – 1037

Vector-based spatial–temporal minimum L1-norm solution for MEG

Ming-Xiong Huang,[a,b,*] Anders M. Dale,[a,c] Tao Song,[a] Eric Halgren,[a] Deborah L. Harrington,[a,d] Igor Podgorny,[a,c] Jose M. Canive,[e,f,g] Stephen Lewis,[e,f,g] and Roland R. Lee [a,b]

[a]*Department of Radiology, University of California, San Diego, San Diego, CA 92037, USA*
[b]*Radiology Service (114), UCSD/VA San Diego Healthcare System, 3350 La Jolla Village Drive, San Diego, CA 92161, USA*
[c]*Department of Neuroscience, University of California, San Diego, San Diego, CA 92037, USA*
[d]*Research Service, VA San Diego Healthcare System, San Diego, CA 92161, USA*
[e]*Center for Functional Brain Imaging, New Mexico VA Health Care System, Albuquerque, NM 87108-5153, USA*
[f]*Department of Psychiatry, University of New Mexico Health Sciences Center, Albuquerque, NM 87131, USA*
[g]*Department of Neurosciences, University of Mexico Health Sciences Center, Albuquerque, NM 87131, USA*

Received 28 July 2005; revised 22 November 2005; accepted 29 January 2006
Available online 15 March 2006

Minimum L1-norm solutions have been used by many investigators to analyze MEG responses because they provide high spatial resolution images. However, conventional minimum L1-norm approaches suffer from instability in spatial construction, and poor smoothness of the reconstructed source time-courses. Activity commonly "jumps" from one grid point to (usually) the neighboring grid points. Equivalently, the time-course of one specific grid point can show substantial "spiky-looking" discontinuity. In the present study, we present a new vector-based spatial–temporal analysis using a L1-minimum-norm (VESTAL). This approach is based on a principle of MEG physics: the magnetic waveforms in sensor-space are linear functions of the source time-courses in the imaging-space. Our computer simulations showed that VESTAL provides good reconstruction of the source amplitude and orientation, with high stability and resolution in both the spatial and temporal domains. "Spiky-looking" discontinuity was not observed in the source time-courses. Importantly, the simulations also showed that VESTAL can resolve sources that are 100% correlated. We then examined the performance of VESTAL in the analysis of human median-nerve MEG responses. The results demonstrated that this method easily distinguishes sources very spatially close to each other, including individual primary somatosensory areas (BA 1, 2, 3b), primary motor area (BA 4), and other regions in the somatosensory system (e.g., BA 5, 7, SII, SMA, and temporal–parietal junction) with high temporal stability and resolution. VESTAL's potential for obtaining information on source extent was also examined.

Keywords: Lead field; MEG; Minimum norm; Spatial–temporal; Median-nerve; L1-norm; Dipole

Introduction

MEG is a functional imaging technique that detects neuronal activity with millisecond temporal resolution. However, many different source configurations can generate identical magnetic field distribution at the MEG sensor array. In order to unambiguously localize the sources that generate the MEG signal, specific assumptions must be made about the nature of the neuronal sources. These are termed "source models." A widely accepted source-modeling technique for MEG involves calculating a set of equivalent current dipoles (ECDs), assuming that the underlying neuronal sources are focal. This dipole fitting procedure is non-linear and over-determined since the number of unknown dipole parameters is much less than the number of MEG measurements. Automated multiple-dipole model algorithms such as multiple signal classification (MUSIC) (Mosher et al., 1992; Mosher and Leahy, 1998; Mosher et al., 1999a) and multistart spatial and temporal (MSST) multiple-dipole modeling (Huang et al., 1998; Aine et al., 2000; Huang et al., 2000; Shih et al., 2000; Stephen et al., 2002; Hanlon et al., 2003; Stephen et al., 2003; Huang et al., 2004a; Huang et al., 2004b) have been studied and applied to the analysis of human MEG responses. However, the ability of dipole models to adequately characterize neuronal responses is limited due to (1) difficulties in localizing extended sources with ECDs; (2) problems in accurately estimating the number of dipoles in advance; and (3) the sensitivity of dipole time-courses to errors in dipole location, particularly in depth.

Other methods of modeling MEG responses include lead-field-based imaging approaches. Unlike multiple-dipole modeling, lead-field approaches divide the source space into a grid containing a large number of dipoles, and the inverse problem is to obtain the dipole moments for the grid nodes (Hamalainen and Ilmoniemi, 1994). Here the inverse solution is a highly under-determined since the number of unknown dipole moments is much greater than the

* Corresponding author. Radiology Service (114), UCSD/VA San Diego Healthcare System, 3350 La Jolla Village Drive, San Diego, CA 92161, USA. Fax: +1 858 552 7404.
E-mail address: mxhuang@ucsd.edu (M.-X. Huang).
Available online on ScienceDirect (www.sciencedirect.com).

1053-8119/$ - see front matter © 2006 Elsevier Inc. All rights reserved.
doi:10.1016/j.neuroimage.2006.01.029

number of MEG sensors. Consequently, a large number of solutions can fit the data equally well. To handle this ambiguity, additional constraints are needed to reduce the non-uniqueness of the solution. The main advantage of lead-field approaches is that the number of sources to model does not need to be specified in advance. The minimum L2-norm inverse is a lead-field-based inverse solution that minimizes the total power (L2-norm) of the dipole moment (Hamalainen and Ilmoniemi, 1994). Such a solution can be easily obtained using a direct linear inverse operator (pseudo inverse calculation with regularization) of the lead fields. Dale et al. (2000) developed an anatomically constrained minimum L2-norm solution using noise covariance normalization to obtain statistical significance of MEG responses. Strengths of this solution included low computational cost and smooth source time-courses, making statistical comparison across different conditions quite simple. This anatomically constrained minimum L2-norm solution has been used in many MEG applications (Dale et al., 2000; Dale and Halgren, 2001; Marinkovic et al., 2003). However, the spatial resolution of the minimum L2-norm solution is relatively low and tends to provide distributed reconstructions even if the true generators are focal. Cross-talk between source time-courses of nearby grid points can also be relatively high.

Independent component analysis (ICA) is another signal processing tool that can separate different signals, which are statistically independent in time. ICA has been used to successfully identify and remove artifacts (e.g., eye blink, eye movement, muscle artifact, cardiac artifact, etc.) from contaminated EEG and MEG data (Vigario, 1997; Ikeda and Toyama, 2000; Jung et al., 2000a; Jung et al., 2000b). ICA has also been used to separate different brain sources (Makeig et al., 1997; Vigario and Oja, 2000; Vigario et al., 2000; Barros et al., 2000; Jung et al., 2001). However, it has been difficult to directly examine two major assumptions underlying ICA: that source time-courses of brain activation are (1) statistically independent, and (2) non-Gaussian. Statistical independence implies uncorrelated source time-courses; ICA has difficulties of resolving highly correlated brain sources.

To address these limitations, the present study examined the efficacy of a novel minimum L1-norm solution in analyzing MEG responses. The minimum L1-norm solution selects the source configuration that minimizes the absolute value of the source strength, and can handle highly correlated sources, since additional assumptions about their temporal dynamics are not needed. Like the minimum L2-norm, the minimum L1-norm method does not need information about the number of sources as a prerequisite. Unlike minimum L2-norm solutions, the minimum L1-norm solution can also provide focal high-resolution images for focal generators. The minimum L1-norm solution is a non-linear minimization approach that can be effectively implemented by linear programming (LP) (Matsuura and Okabe, 1995; Matsuura and Okabe, 1997; Uutela et al., 1999). Although LP is not as fast as the direct pseudo-inverse used by the minimum L2-norm solution, many LP algorithms can efficiently handle problems with thousands to millions of variables. Deviating from the LP implementation of minimum L1-norm approaches, Phillips et al. (1997) suggested a lead-field-based inverse method for MEG using a combination of L1-norm and neighborhood clustering function. However, their cost function needed to be minimized by a Markov random field (Geman and Geman, 1984), which results in a high computational cost, particularly when the number of dipoles on the grid is large.

Although minimum L1-norm methods, particularly the magnetic current estimation (MCE) L1-norm solution (Uutela et al., 1999), have been used in many MEG applications (Vanni and Uutela, 2000; Tesche, 2000; Stenbacka et al., 2002; Pulvermuller et al., 2003; Osipova et al., 2005; Auranen et al., 2005; Liljestrom et al., 2005), these conventional approaches have some limitations. The first is that the dipole orientation at each grid point must be known before applying L1-norm methods (Uutela et al., 1999); or the dipole orientation must be iteratively determined (Matsuura and Okabe, 1995, 1999). The latter approach can significantly slow down the computation, without appreciably improving the results (Uutela et al., 1999). In the former case, the dipole orientation on each grid point is chosen based on the orientation derived from the minimum L2-norm approach. However, when MEG data contain multiple generators, the L2-norm reconstructed dipole orientation may deviate from the true orientation (see Results for examples), which can then cause the minimum L1-norm analysis to misfit the data.

The most serious limitations of conventional minimum L1-norm approaches are their instability in spatial location and poor smoothness in reconstructed source time-courses. For instance, one often sees activity "jumping" from one grid point to (usually) neighboring grid points. Equivalently, the time-course of one specific grid point can show substantial "spiky-looking" discontinuities. This problem is also encountered in other focal localization methods using lead-field approaches (e.g., FOCUSS Gorodnitsky et al., 1995). Although averaging across many time points reduces the discontinuity in source time-courses, this results in a loss in temporal resolution (Uutela et al., 1999; Vanni and Uutela, 2000; Tesche, 2000; Stenbacka et al., 2002; Pulvermuller et al., 2003; Osipova et al., 2005; Auranen et al., 2005; Liljestrom et al., 2005).

In the present study, we introduce a novel vector-based *spatial–temporal* analysis using a L1-minimum-norm (VESTAL) solution. This approach is to ensure the linear relationship between MEG waveforms in sensors and the time-courses of the underlying neuronal sources. In the VESTAL approach, the temporal information in the data was used to enhance the stability of the reconstructed vector-based L1-minimum norm solution. Since this approach makes no additional assumptions about the temporal dynamics of the sources, it can also handle sources that are 100% correlated. VESTAL also effectively obtains source strength and dipole orientation without iteration or choosing a pre-fixed dipole orientation for each grid node. VESTAL was tested in computer simulations, and using data from human MEG responses. The results show that VESTAL provides high spatial stability and continuous temporal dynamics, without compromising spatial or temporal resolution.

Material and methods

Minimum L1-norm solution (general approach)

As in all lead-field-based MEG and EEG inverse approaches, we first divide the source space (the brain volume or just the cortex) into a grid of a large number of dipole locations. The $m \times s$ sensor waveform matrix $\mathbf{B} = [\boldsymbol{b}(t_1), \boldsymbol{b}(t_2), \ldots, \boldsymbol{b}(t_s)]$ contains MEG data where m is the number of MEG sensors and s is the number of time points, $\boldsymbol{b}(t_i)$ is an $m \times 1$ vector of the MEG measurements at given time point. For each column of $\mathbf{B}$, we have:

$$\boldsymbol{b} = \mathbf{G}\boldsymbol{q} + \text{noise} \quad (1)$$

where $\mathbf{G}$ is the $m \times n$ (lead-field) gain matrix, $\boldsymbol{q}$ is the $n \times 1$ dipole moment vector for given time point, and n is the number of

unknown dipole moment parameters related to the number of points p in the source grid. In general, $n = 3p$ if all x, y, and z components (or ρ, θ, φ components in spherical coordinate system) of the dipole moment contribute to the MEG field. If one used a spherical MEG head model, the radial (ρ) component of the dipole generates zero external magnetic fields and $n = 2p$. In the case that the dipole orientation is known or pre-fixed, $n = p$. The MEG inverse problem is to obtain $\boldsymbol{q}$ for a given $\boldsymbol{b}$. Since m (the number of equations) is usually much less than n (the number of unknown parameters), we are dealing with a highly under-determined problem, and there are a large number of solutions that will fit the data. To reduce the ambiguity, additional constraints (source models) are needed. The minimum L1-norm solution selects the source configuration that minimizes the absolute value of the source strength. Let $\mathbf{G} = \mathbf{USV}^T$ be the singular value decomposition of the gain matrix, the minimum L1-norm solution is seeking the source distribution $\boldsymbol{q}$ that meets the following condition (Uutela et al., 1999):

$$\min\left(\mathbf{w}^T|\boldsymbol{q}|\right) \quad \text{subject to constraints } \mathbf{S}_{\mathrm{ng}}\mathbf{V}_{\mathrm{ng}}^T\boldsymbol{q} \cong \mathbf{U}_{\mathrm{ng}}^T\boldsymbol{b} \tag{2}$$

where $\mathbf{S}_{\mathrm{ng}}$, $\mathbf{U}_{\mathrm{ng}}$, and $\mathbf{V}_{\mathrm{ng}}$ contain the ng largest singular values and the associated singular vectors, respectively. In Eq. (2), $\boldsymbol{w}$ is an $n \times 1$ optional weighting vector chosen to remove potential bias towards grid nodes at the superficial layer and it usually taken to be the column norm of the $\mathbf{G}$ matrix (Matsuura and Okabe, 1997; Uutela et al., 1999) or a Gaussian function (Ioannides et al., 1993). Unlike the minimum L2-norm solution, the solution to Eq. (2) is a non-linear minimization procedure. However, if one can replace the absolute values in $|\boldsymbol{q}|$ with some non-negative values related to $\boldsymbol{q}$, one can solved the set of equations through (primal) linear programming (LP).

Because the dipole moments can be either positive or negative, an additional step is needed to deal with the absolute values. It has been proposed that if one introduces two new non-negative variables $\boldsymbol{q}^a$ and $\boldsymbol{q}^b$ (Eiselt et al., 1987), one can rewrite Eq. (2) as:

$$\begin{aligned}\min\left(\boldsymbol{w}^T\left(\boldsymbol{q}^a + \boldsymbol{q}^b\right)\right)\text{s.t. } \mathbf{S}_{\mathrm{ng}}\mathbf{V}_{\mathrm{ng}}^T\boldsymbol{q} \cong \mathbf{U}_{\mathrm{ng}}^T\boldsymbol{b}, \boldsymbol{q} = \boldsymbol{q}^a \\ - \boldsymbol{q}^b, \left\{\boldsymbol{q}_j^a\right\}, \left\{\boldsymbol{q}_j^b\right\} \geq 0, \{q_j\}, j = 1{:}n\end{aligned} \tag{2a}$$

On the other hand, one can also introduce a different non-negative variable r (Chvatal, 1983; Eiselt et al., 1987; Matsuura and Okabe, 1997), such that Eq. (2) can be rewritten as:

$$\min\left(\boldsymbol{w}^T r\right)\text{s.t. } \mathbf{S}_{\mathrm{ng}}\mathbf{V}_{\mathrm{ng}}^T\boldsymbol{q} \cong \mathbf{U}_{\mathrm{ng}}^T\boldsymbol{b}, \boldsymbol{q} \leq r, \boldsymbol{q} \geq -r, r \geq 0 \tag{2b}$$

The drawback of both of these two approaches is the substantial increase in the number of variables and constraints (Eiselt et al., 1987). Two alternative approaches were introduced to handle this issue, both of which required knowledge of the dipole orientation at each grid node. The first approach by Matsuura and Okabe (1999) who modified the LP algorithm to iteratively update the orientation. However, partially due to convergence problems, the results did not appear substantially better than a second approach by Uutela et al. (1999) who pre-fixed each dipole orientation to the one obtained from a minimum L2-norm solution. In both cases, minimizing the L1-norm was transferred into minimizing the sum of non-negative dipole amplitudes through LP. Such approaches may cause a misfit of the data if the orientation derived from iteration or the minimum L2-norm solution deviates from the real orientation when multiple sources are activated at the same time (see Results).

New vector-based minimum L1-norm solution

In the present study, we adopted a vector-based minimum L1-norm approach, which deals with all $n = 3p$ (or $2p$ in the case of MEG spherical model) dipole components individually. We found that in order to handle the non-negative requirement of the LP, we only needed to know the sign of each component at each grid node, not the actual orientation of the dipole. Assuming we have such information about the sign, we will have:

$$\min\left(\boldsymbol{w}^T\boldsymbol{d}\right), \quad \text{subject to constraints } \mathbf{S}_{\mathrm{ng}}\mathbf{V}_{\mathrm{ng}}^T\boldsymbol{\Omega}\boldsymbol{d} \cong \mathbf{U}_{\mathrm{ng}}^T\boldsymbol{b} \tag{3}$$

where $\boldsymbol{d}$ is a $n \times 1$ non-negative dipole strength vector and $\boldsymbol{\Omega}$ is a $n \times n$ diagonal sign matrix with the diagonal elements equal ± 1 dependent on the sign of the dipole moments (in x, y, z or ρ, θ, φ directions) at each grid node. Eq. (3) can be easily solved by LP. The remaining problem is to obtain the sign information for each component of the dipole moment at each grid node. In practice, we found that the sign information from the minimum L2-norm solution is adequate to construct the $\boldsymbol{\Omega}$ matrix. Note that unlike the approach from Uutela et al. (1999) who pre-fixed the orientation of the dipole to the one obtained from the L2-norm solution (i.e., fixed the ratio of the x, y, and z components of each dipole moment), we only adopted the sign of each component from the L2-norm solution without imposing constrains on the ratios between x, y, or z components. This is one difference between our vector-based minimum L1-norm approach and conventional L1-norm approaches, which allow us to reconstruct not only the dipole strength, but also the dipole orientation as shown in the simulation (see Results). Our experience also suggests that this new vector-based L1-minimum-norm approach using Eq. (3) gives virtually the same result, with only a fraction of computational cost, as the approach using Eqs. (2a) or (2b).

Handling the orientation bias towards the coordinate axes

One problem that needs to be addressed by the minimum L1-norm approach is that the solution has a tendency (bias) towards the coordinate axes. For example, in spherical MEG head model, a dipole at the ith node of the grid, the vector-based L1-minimum norm solution can also be expressed as minimizing $\sum_{i=1}^{p}\boldsymbol{w}_i d_i$ $(|\cos(\psi_i)| + |\sin(\psi_i)|)$ where ψ_i is the angle between total dipole moment and the orientation of the elevation in a tangential containing the dipole node, and d_i is the non-negative dipole strength. This will introduce a bias towards the coordinate axes (Fig. 1). In order to handle this bias, an additional factor $\left(|\cos\left(\psi_i^e\right)| + |\sin\left(\psi_i^e\right)|\right)^{-1}$ was included in the weighting vector $\boldsymbol{w}$ in Eq. (3), where ψ_i^e is the angle associated with the estimated orientation based on L2-minim norm solution. Notice that we only used the orientation estimation from the L2-norm to reduce the bias for the L1-norm analysis, but did not force the L1-norm solution to be in the L2-norm orientation. The results from the simulations showed that the L1-norm orientation obtained using this approach is more accurate than the original estimation of the orientation from L2-norm.

Another advantage of the above approach is that one does not need to worry about the convergence problem in a separate orientation optimization step (Matsuura and Okabe, 1999). We found that this process can be time-consuming and becomes impractical for a grid with a large number of dipoles. With the new approach of using the estimated L2-norm orientation in the

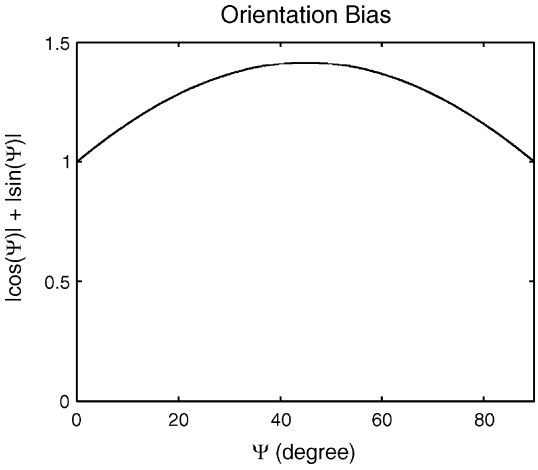

Fig. 1. Orientation bias of the minimum L1-norm solution. A spherical MEG model is assumed. Here, ψ measures the angle between the total dipole moment vector and the orientation axes. $\psi = 0°$ means the dipole moment vector is along the orientation of elevation (i.e., $\hat{\theta}$), while $\psi = 90°$ indicates the dipole points to the azimuth direction (i.e., $\hat{\varphi}$). The function $|\cos(\psi)| + |\sin(\psi)|$ in the L1-norm showed bias (smaller values) towards the coordinate axes.

weighting vector, we were able to achieve accurate orientation with virtually no increase of computational cost.

Handling pink noise with pre-whitening

So far, we are dealing with white noise, which is identical and has an independent distribution (IID). In studying human MEG and EEG responses, correlated pink noise is common. In that case, one needs to perform pre-whitening to the data using the noise covariance matrix $\mathbf{C}$ (Sekihara et al., 1997, 1999), prior to applying the vector-based minimum L1-norm solution. During the process, one can simply replace $\mathbf{G}$ with $\tilde{\mathrm{G}} = \mathbf{C}^{-1/2}\,\mathbf{G}$ and $\mathbf{B}$ (or $\boldsymbol{b}$) with $\tilde{\mathrm{B}} = \mathbf{C}^{-1/2}\,\mathbf{B}$ (or $\tilde{b} = \mathbf{C}^{-1/2}\boldsymbol{b}$). Here, the whitening operator was obtained with the help of the eigenvalue decomposition of the noise covariance matrix: $\mathbf{C} = \mathbf{U}_C\boldsymbol{\Sigma}_C^2\mathbf{U}_C^T$ and $\mathbf{C}^{-1/2} = \boldsymbol{\Sigma}_C^{-2}\mathbf{U}_C^T$ (Hamalainen, 2005). For evoked responses requiring trial averaging, the covariance matrix was obtained from the raw (unaveraged) data, and the covariance matrix of the averaged responses from the raw noise covariance matrix divided by the number of trials used in the averaging (Sekihara et al., 1999; Hamalainen, 2005).

Preventing under- and over-fitting of the data using chi-square

One important issue is to ensure the data are fit appropriately and to prevent over- and under-fitting while minimizing the L1-norm. This is achieved by selecting the appropriate number of dominating singular values ng in Eq. (3). If the selection of ng is too small, one will not be able to fit the data well. On the other hand, if ng is too large, one will actually over-fit the data by fitting the noise feature. In the present approach, we select ng such that the chi-squired value:

$$X^2 = \left(\tilde{\mathbf{G}}p - \tilde{\boldsymbol{b}}\right)^T\left(\tilde{\mathbf{G}}p - \tilde{\boldsymbol{b}}\right) \tag{4}$$

(i.e., the square error between the predicted and measured magnetic fields, divided by the noise covariance matrix) for each time point will be in the range of $m \pm 3.29\sqrt{m}$ where m is the number of MEG/EEG sensors. Statistically, the largest 99% acceptable value for chi-square should be within this range. To fulfill Eq. (4), we explored two approaches to truncate the small singular values in $\tilde{\mathrm{G}}$. The first approach truncated the singular values if they meet the following condition:

$$\lambda_k^2 \le \frac{\alpha}{m}\ \mathrm{Trace}\left(\tilde{\mathbf{G}}\tilde{\mathbf{G}}^T\right)\cdot\frac{1}{\mathrm{SNR}} \tag{5}$$

where λ_k was the singular values of whitened gain matrix $\tilde{\mathrm{G}}$, SNR is the (variance) signal-to-noise ratio of the whitened data, and α is a scaling factor. Such selection was consistent with the one typically used in minimum L2-norm regularization (Hamalainen, 2005). The second approach for truncation used an automated, but more complicated algorithm to determine the optimal truncation based on original work from (Sano, 1993). Our experience showed that both approaches gave satisfactory and very similar results.

New vector-based spatial–temporal analysis using L1- minimum-norm (VESTAL)

One major problem of conventional L1-norm approaches is the instability in spatial construction and discontinuity in reconstructed source time-courses. Vector-based minimum L1-norm solution operating on individual time points will also suffer from the same instability as the conventional approaches. To increase spatial and temporal stability, we developed a spatial–temporal vector-based minimum L1-norm solution. The idea was based on a principle of MEG physics, which states that the magnetic waveforms in the sensor-space are linear functions of the dipole time-courses in the source-space. If we perform singular value decomposition for the $m \times s$ MEG sensor waveform data matrix:

$$\mathbf{B} = \mathbf{U}_B\mathbf{S}_B\mathbf{V}_B^T \tag{6}$$

one can see that all temporal information in the MEG sensor waveform can be represented as a linear combination of the singular vectors in the matrix $\mathbf{V}_B$. Since MEG sensor waveforms are linear functions of the underlying neuronal source time-courses, the same signal subspace that expands the temporal dimension of $\mathbf{B}$ should also expand the temporal dimension of the $n \times s$ source time-course matrix $\mathbf{D} = [\boldsymbol{d}(t_1), \boldsymbol{d}(t_2), \ldots, \boldsymbol{d}(t_s)]$ estimated from the vector-based minimum L1-norm solution for s time points. By projecting $\mathbf{D}$ towards $\mathbf{V}_B$, we can ensure that source time-courses matrix $\mathbf{D}$ and sensor waveform matrix $\mathbf{B}$ share the same temporal information as requested by the MEG physics:

$$\mathbf{D}_{\mathrm{VESTAL}} = \mathbf{D}\mathbf{P}_{||} \tag{7}$$

where the projection matrix $\mathbf{P}_{||} = \mathbf{V}_B\mathbf{V}_B^T$ is constructed using the dominant (signal-related) temporal singular vectors (subspace) of the sensor waveforms. We called $\mathbf{D}_{\mathrm{VESTAL}}$ the vector-based spatial–temporal analysis using L1- minimum-norm (VESTAL). The criterion of selecting the signal-related subspace dimension of the $\mathbf{B}$ matrix through SVD is to make sure the chi-square values stay within the range of $m \pm 3.29\sqrt{m}$ (m is the number of MEG channels) for each time point after the spatiotemporal linear projection using Eq. (7). The adequate subspace dimension is the lowest value that meets this criterion. If the signal-related subspace is under-estimated (i.e., less than the adequate subspace dimension), chi-square values increase dramatically above the upper range. This is as a strong indication of a bad fit and should be avoided. On the other hand, if the signal subspace is over estimated by one or two, the results of the source time-courses and the chi-square values stay virtually the same. This is because the

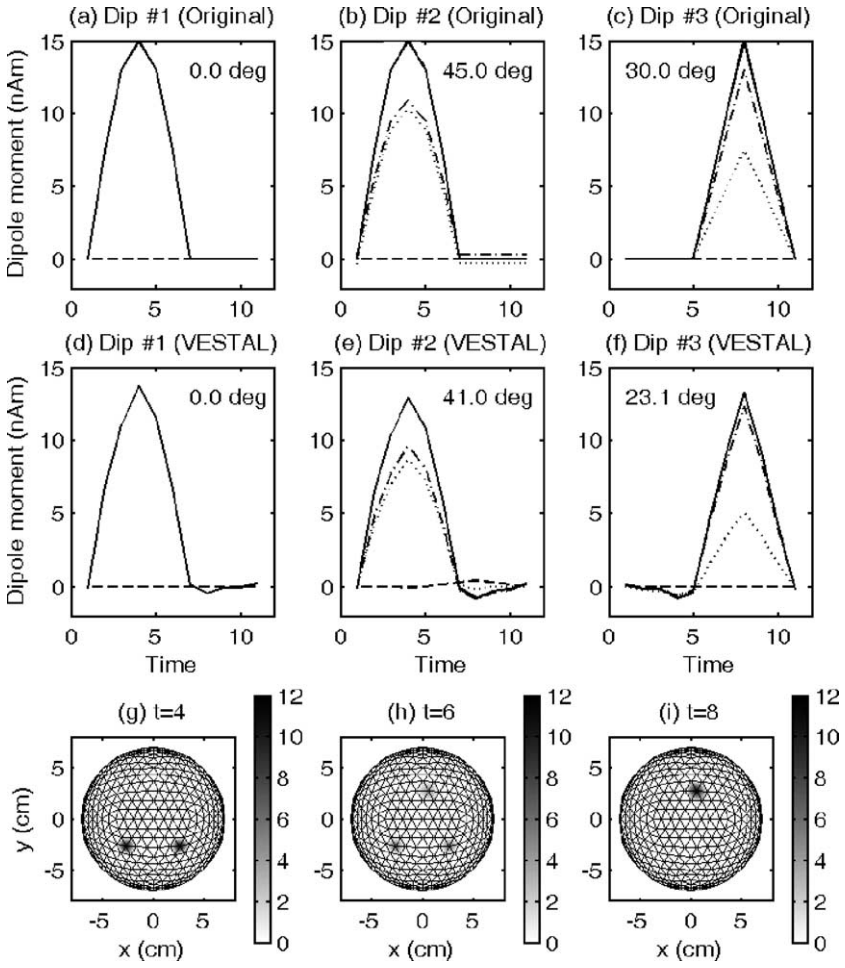

Fig. 2. Computer simulation of VESTAL for 3 dipoles. White noise of 10 fT was added to the sensor waveforms (SNR = 8.1 dB). (a–c) True dipole time-courses for two 100% correlated dipoles (#1 and #2) and one asynchronous dipole (#3). The solid and dashed lines represent the dipole time-courses along the true dipole orientation and the one in the orthogonal direction, respectively. The dashed-dotted line and the dotted line are dipole time-courses along the two coordinate axes (i.e., $\hat{\theta}$ and $\hat{\varphi}$). The three numbers in each subplot indicate the angle between the total dipole moment vector and the direction of $\hat{\theta}$. (d–f) Reconstructed dipole time-courses using VESTAL. The solid and dashed lines represent the dipole time-courses along the best fitting dipole orientation and the one in the orthogonal direction, respectively. The other definitions are the same as in the first row. (g–i) Source strength maps of VESTAL at three time points. The three black spots from VESTAL coincide with the true dipole locations.

probability that spatiotemporal modes of the signal fall into the few noise singular vectors by chance (due to slightly over-estimation) is rather small. Insensitivity to slight over-estimations of the subspace dimension has been observed in other MEG inverse approaches as well (e.g., MUSIC: Mosher et al., 1992; Mosher and Leahy, 1998).

In many cases, researchers want to obtain the best fitting orientation and source time-courses associated with the best orientation. In the present study, the best fitting orientation *at each node* is obtained by simply adopting the orientation of the leading spatial-domain (row or left) singular vector formed by the time-courses of the individual components of the dipole at the node. The associated best fitting source time-course is the leading time-domain (column or right) singular vector multiplied by the leading singular value (Mosher et al., 1992; Mosher and Leahy, 1998).

Setup for computer simulations and analyzing human MEG response

In the present study, two computer simulations were conducted to examine three key issues related to the performance of VESTAL. These issues included: (1) examining VESTAL's ability of handling highly correlated sources, (2) studying VESTAL's accuracy of obtaining source orientations when the true orientations is along the coordinate axes or deviate from them, and (3) exploring VESTAL's potential of obtaining source extent and the impact of the upper limit of the source amplitude to the source extents.

The performance of VESTAL was further examined using human MEG responses evoked by unilateral median-nerve stimulation. This task is particularly appropriate because it has been used routinely in humans to study the somatosensory system, which is probably the most well studied neuronal system in humans. Consequently, we have an excellent understanding of the underlying neuronal activity, which allowed us to predict with a high degree of confidence where sources should be found. For example, neurophysiology studies have shown that strong stimulation of the peripheral nerve activates: (1) primary somatosensory area (SI) with a first component around 20 ms post-stimulus (Wood et al., 1985; Hari et al., 1993; Forss et al., 1994; Kawamura et al., 1996; Mauguiere et al., 1997a,b; Jousmaki and Forss, 1998; Forss and Jousmaki, 1998; Hari and Forss, 1999; Huang et al., 2000,

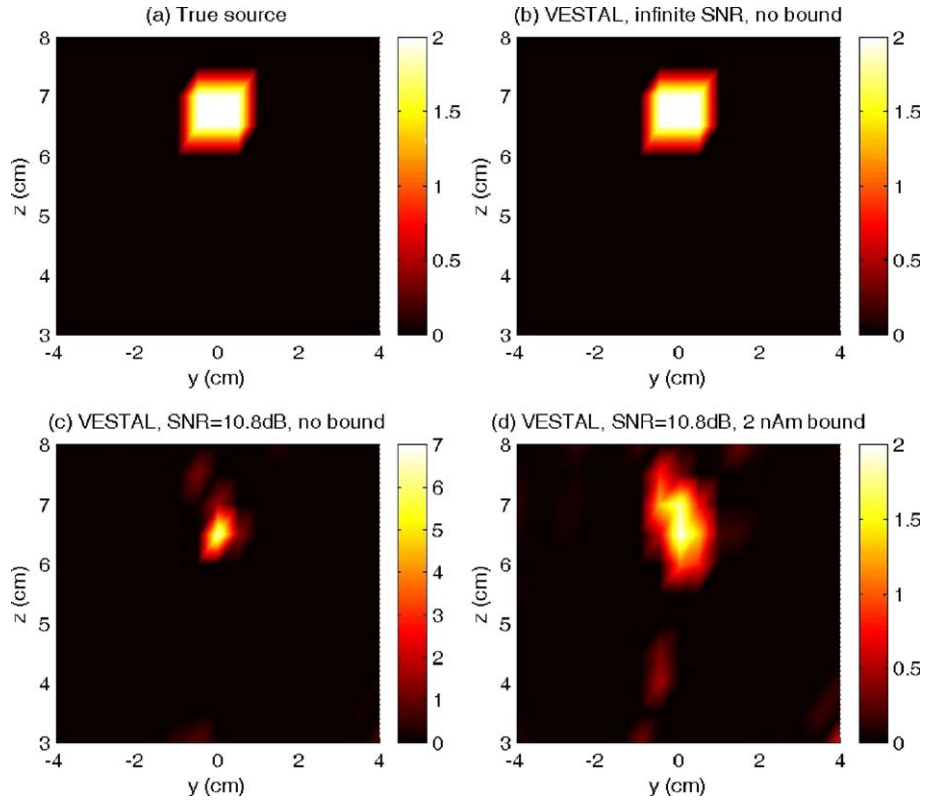

Fig. 3. Computer simulation of VESTAL for obtaining source extent. (a) The true source configuration with extent. (b) Under a very high SNR condition (70 dB $\sim \infty$) with no upper bound imposed on source strength, VESTAL accurately reconstructs the source geometry. (c) Under a more realistic SNR level where the difference between the MEG fields generated by the true source and the point focal source is less than the noise level, VESTAL provides a focal reconstruction with stronger amplitude. Here, no upper bound is imposed on the source strength, which explains the large difference in the scaling on the color bar. (d) When we impose an upper bound to the source amplitude, VESTAL provides a source extent comparable to the true source.

2004a, 2005); (2) primary motor area (M1) with a first component around 20–30 ms post-stimulus (Rosen and Asanuma, 1972; Lemon and Porter, 1976; Jones et al., 1978; Wong et al., 1978; Jones et al., 1979; Lemon, 1979; Lemon, 1981; Davidoff, 1990; Baldissera and Leocani, 1995; Kawamura et al., 1996; Spiegel et al., 1999; Huang et al., 2000; Huang et al., 2004a; Huang et al., 2005); (3) superior parietal area (Jones et al., 1978; Jones et al., 1979; Forss et al., 1994; Boakye et al., 2000; McGlone et al., 2002; Waberski et al., 2002); (4) supplementary motor area or SMA (Urbano et al., 1997; Boakye et al., 2000; Barba et al., 2001); and (5) secondary somatosensory areas (SII) (Hari et al., 1993; Forss and Jousmaki, 1998; Hari and Forss, 1999; Fujiwara et al., 2002; Simoes et al., 2003; Huang et al., 2005).

However, in previous MEG studies, it has proven difficult to distinguish individual regions in SI (BA 1, 2, and 3b) and the parietal cortex (BA 5 and 7), which is part of the somatosensory system (Kandel et al., 2000). In addition, we are not aware of any study that has shown source time-courses for all of these regions at once.

A data set of this kind is quite challenging for many MEG inverse algorithms since it contains a large number of neuronal generators, many of which are very close in space. Additional complications are that sources can be both focal and extended, have a relatively short duration in time, and may have highly correlated time-courses. This type of challenge is especially suitable for evaluating the strengths of VESTAL.

To evaluate VESTAL using a challenging data set, we conducted MEG recordings from a healthy subject as he underwent median-nerve stimulation. The subject's right median-nerve was stimulated using a bipolar Grass™ constant current stimulator. The stimuli were square-wave electric pulses (0.2 ms duration) delivered at about 1 Hz (ISI: 800 ms to 1200 ms). The intensity of the stimulation was adjusted until robust thumb twitches were observed. A trigger from the stimulator, which was simultaneous with the stimulus, was sent to the MEG acquisition system for signal averaging. Magnetic fields evoked by median-nerve stimulation were measured using an Elekta/Neuromag™ whole-head MEG system (Helsinki, Finland), with 122 planar gradiometer channels in a magnetically shielded room (IMEDCO-AG, Switzerland). EOG electrodes were used to detect eye blinks and eye movements. An interval of 500 ms post-stimulus was recorded, using 300 ms pre-stimulus data for noise estimation. Data were sampled at 1000 Hz and run through a high-pass filter with 0.1 Hz cut-off and through a notch filter (58–62 Hz) to remove 60 Hz power-line noise. Three hundred artifact-free MEG responses were averaged with respect to the stimulus trigger to increase the SNR.

Results

Computer simulations examining the performance of VESTAL

Example one: focal and 100% correlated sources

The purposes of the first simulation are: (1) to examine the ability of the VESTAL method in providing high spatial and

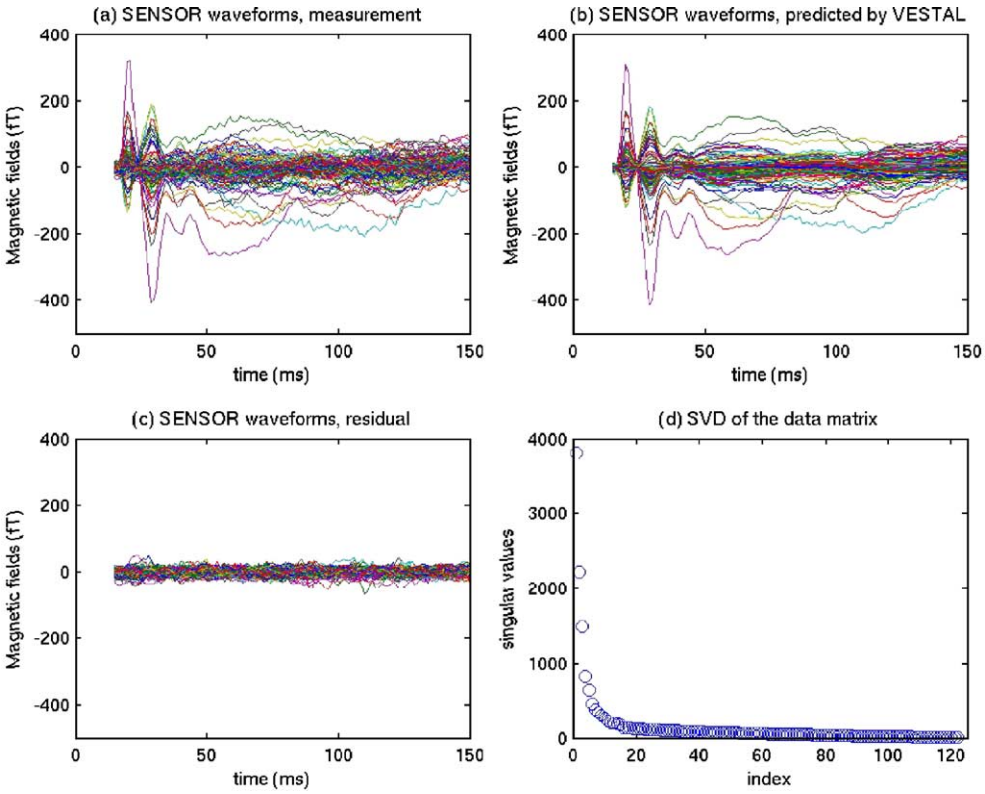

Fig. 4. Superimposed MEG sensor waveforms evoked by right median-nerve stimulation in a normal subject. (a) Measured sensor waveforms. (b) Predicted sensor waveforms from VESTAL. (c) Residual waveforms. (d) Singular values of the measured sensor waveforms.

temporal stability when handling focal and correlated sources, even in a noisy environment and (2) to examine the accuracy of obtaining the source orientation using VESTAL. Simulated MEG responses were generated with 3 dipoles, two of which had time-courses that were correlated 100% (Figs. 2a–c). A spherical head model was used in the forward calculation (Sarvas, 1987). In this head model, only the two tangential dipole components were used in the calculation since radial components of a dipole do not contribute to the MEG fields. The orientation of the dipoles was designed to cover a variety of situations: Dipole #1 (Fig. 2a) was along one coordinate axes in the elevation direction $\hat{\theta}$; Dipole #2 (Fig. 2(b)) was 45° from both coordinate axes (i.e., $\hat{\theta}$ and azimuth direction $\hat{\varphi}$), and Dipole #3 (Fig. 2c) was 30° from $\hat{\theta}$ and 60° from $\hat{\varphi}$. In Fig. 2(b), the time-courses along were artificially displaced up-and-down a little for visualization purpose. The sensor configuration of an Elekta/Neuromag™ whole-head 122-channel MEG system was adopted in the simulation. White noise with 10 fT SD was added to the sensor waveforms. The total noise variance was 15% of the signal variance for the entire interval (SNR = 8.1 dB).

The inverse solution using VESTAL with a spherical grid (642 vertices) showed that the algorithm had no problem accurately localizing these dipoles. Figs. 2d–f showed that VESTAL accurately reconstructed the shape of dipole time-courses, including ones that were 100% correlated (Figs. 2d–f). No "spiky-looking" discontinuities (a typical phenomenon of conventional minimum L1-norm approaches) were observed. The reconstructed dipole orientations from VESTAL deviated from the true orientations by 0.0°, 4.0°, and 6.9°, respectively.

In contrast, the orientations obtained from the minimum L2-norm solution deviated from the true dipole orientations by 10.3°, 12.5°, and 11.1°, respectively for the three grid nodes where the true dipoles are located. This result demonstrates that the dipole orientations from VESTAL were more accurate than the ones provided by minimum L2-norm solution.

Example two, source extent

The second example explored VESTAL's performance in obtaining the spatial extent of the source. A cubic grid of 5 mm mesh size was used in the simulation. Fig. 3a shows the true source configuration in which 6 grid points were activated simultaneously to generate the signal. A half sinusoidal time-course with a maximum amplitude of 2 nAm was used by all the nodes that were active. For a nearly noiseless case (SNR $\sim \infty$ (70 dB)) with no upper bound imposed on the source strength, VETSAL precisely reconstructed the shape of the source (Fig. 3b). However, when a realistic amount of noise (SNR = 10.8 dB) was added to the data without an upper bound on source strength, VESTAL showed a more focal reconstruction than the true source configuration, but with a much stronger amplitude (i.e., ~7 nAm in Fig. 3c; note the difference in scaling of the color bar) than any of the individual nodes in the true configuration. The reason for this phenomenon is well-known: the difference in the magnetic fields created by the source configurations in Figs. 3a and c is much less than the noise variance, a typical example of the ill-posed problem of the MEG inverse solution. VESTAL simply chose the focal source configuration that fit the data. On the other hand, when we put an upper bound

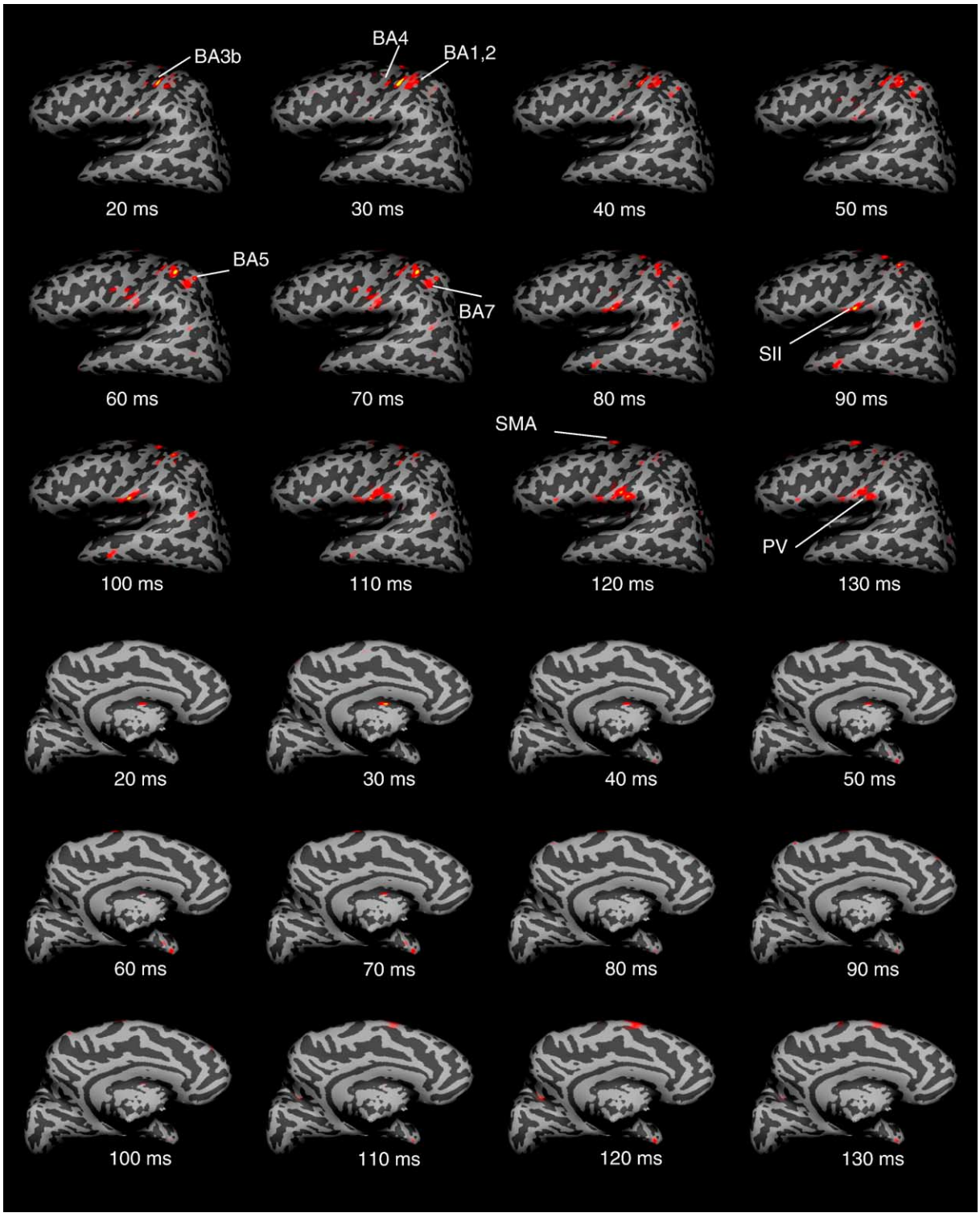

Fig. 5. Snapshots of VESTAL source amplitudes across time in the left hemisphere viewed from lateral (top three rows) and medial (bottom three rows) directions. Sources were obtained from MEG responses evoked by right median-nerve stimulation in a healthy subject. The color scale (opaque red to bright yellow) was from 0 nAm to 5 nAm. Top two rows: early activations of individual areas in SI (BA, 1, 2, and 3b) and M1 (BA 4) were highly distinguishable. BA 5 and 7 showed activation during 40–70 ms. Middle two rows: SII, PV, SMA, anterior temporal, and temporal–parietal junction showed activation later than the primary sensorimotor areas. Bottom rows: an area in the vicinity of the thalamus showed early activation.

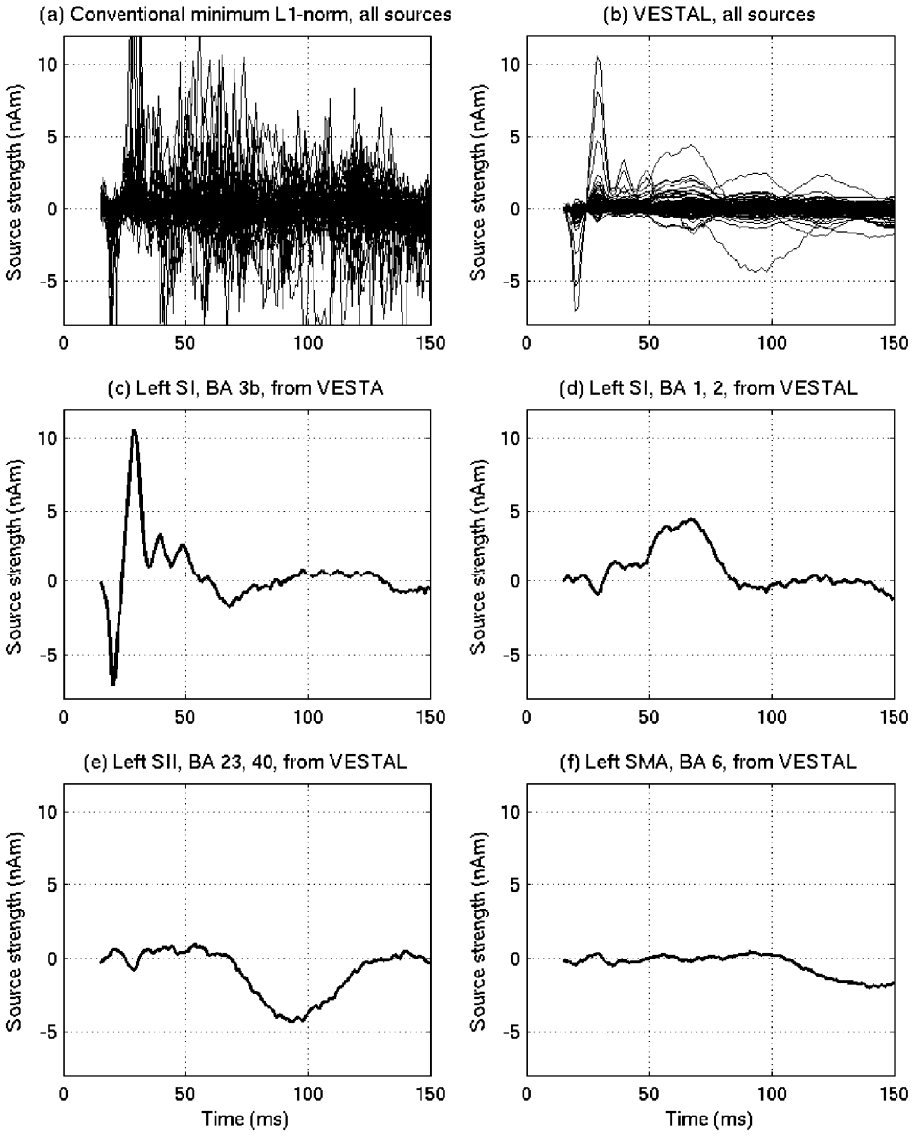

Fig. 6. Marked improvement of the smoothness for the source time-courses of the median-nerve responses using VESTAL. (a) Superimposed "spike-looking" source time-courses when conventional minimum L1-norm was used to fit the median-nerve response. (b) Superimposed source time-courses after the spatiotemporal projection using VESTAL. The rest showed four individual source time-courses from VESTAL: (c) SI BA 3b; (d) SI BA 1, 2; (e) SII BA 23, 40; (f) SMA, BA 6.

on the source amplitude (Fig. 3d; 2 nAm bound), VESTAL shows a source extent that is more comparable with the true source configuration.

Performance of VESTAL for human MEG responses

The VESTAL approach was applied to a data set containing MEG responses evoked by unilateral median-nerve stimulation in a healthy subject. Fig. 4a shows the measured sensor waveforms of MEG responses evoked by the right median-nerve stimulation, with all 122 channels superimposed. The predicted MEG sensor waveforms in Fig. 4b from the VESTAL solution matched the measurement very well. Fig. 4c shows that mainly noise remained in the residual waveforms (i.e., measurement minus predicted). The singular values of the sensor waveforms in Fig. 4(a) are displayed in Fig. 4d. A subspace of dimension six was used by VESTAL for spatial–temporal projection in Eq. (7).

Fig. 5 shows multiple snap shots across time of the VESTAL solution. No threshold was applied to the maps due to the clean background in the VESTAL reconstruction. The inflated brain surface was obtained using the Freesurfer software (Dale et al., 1999; Fischl et al., 2004). In this analysis, a grid containing 7757 nodes was used as the source space for the cortical region, plus 1058 nodes for the cerebellum. The boundary element method (BEM) (Hamalainen and Sarvas, 1989; Ferguson et al., 1994; Schlitt et al., 1995; Mosher et al., 1999b) was used as the forward model. For each node, the two dominant components (essentially the two tangential components) were used in the analysis so that the total number of unknown variables was 17630 per time point.

Fig. 5 displays snapshots of VESTAL derived source amplitudes across time in the left lateral (top three rows) and medial (bottom three rows) views of the left hemisphere. During the 20–30 ms interval, primary somatosensory (SI) and primary motor (MI) areas were activated with the dominant activation in BA 3b and weaker

activation in BA 1, 2, and 4. During the 50–70 ms interval, activation in BA 3b decreased while BA 1 and 2 become the dominant sources. Another interesting finding was the ability of VESTAL to map out BA 5 and 7. These two areas became activated at 40 ms and activity lasted until around 80 ms. Activation of the secondary somatosensory area (SII, BA 23/40) started after 60 ms and peaked about 90 ms. Another noteworthy finding was that a region in the ventral parietal (PV) area slightly poster to SII became activated at about 110 ms. A couple of sources in the temporal lobe were also observed. The temporal–parietal junction, a poly-sensory area, was activated between 70 ms and 110 ms. Another more anterior temporal area showed activation between 80 and 110 ms. SMA activity is also visible in Fig. 5, but it started relatively late at about 110 ms and peaked at about 130 ms. In addition to the cortical areas, early activation was seen in the thalamus (row 4 in Fig. 5). The cerebellum is not shown in the plot since the highest amplitude observed in that region was only 0.55 nAm.

Fig. 6 demonstrates the marked improvement of the smoothness for the source time-courses using VESTAL. Fig. 6a shows the superimposed source time-courses when the conventional minimum L1-norm was used to fit the same median-nerve response. The solution was sensitive to noise and "Spiky-looking" discontinuities were highly visible. Fig. 6b shows the superimposed source time-courses after the spatiotemporal projection using VESTAL (Eq. (7)). The "spiky-looking" discontinuities were absent in the VESTAL source time-courses which were as smooth as the sensor waveforms in Fig. 4a. The remaining of the plots in Fig. 6 show the time-courses of four individual neuronal generators obtained by VESTAL. The SI (BA 3b) sources in Fig. 6c showed strong activation during 20–30 ms. The SI (BA 1, 2) source time-course clearly showed a broad peak during 50 ms–80 ms and peaked at about 65 ms (Fig. 6(d)). The SII area started at about 65 ms, peaked at about 90 ms, and ended at about 120 ms (Fig. 6e). In contrast, the much later SMA generator started at about 100 ms and peaked at about 130 ms (Fig. 6f).

Computational cost of VESTAL

The computational cost of VESTAL is low compared with many non-linear optimization approaches such as non-linear multiple-dipole modeling (Huang et al., 1998). In the above example of human median-nerve MEG responses using a grid of 8815 nodes and 17630 dipole moment parameters per time point, it took about 23 s to finish the fit for each time point. The total time for the entire interval with 136 time points was about 50 min. The LP calculation was performed using the "linprog" program in the MATLAB™ Optimization Toolbox on a LINUX-based PC from Dell with Intel 3.2 GHz Xeon™ CPU and 1 GB RAM.

Discussion

In the present study, a new vector-based spatial–temporal analysis using L1-minimum-norm or VESTAL was studied. Computer simulations and results from analyses of human MEG responses showed several advantages of this novel algorithm. First, VESTAL has high stability and resolution in the spatial domain. This was particularly striking in the analysis of the median-nerve stimulation data, which illustrated that VESTAL can easily distinguish sources that are very close spatially, such as primary somatosensory areas BA 1, 2, 3b, and primary motor area BA 4. Second, VESTAL also demonstrated high stability and resolution in the temporal domain. Figs. 6(a) and (b) clearly showed the dramatic improvement of the temporal continuity using VESTAL over the conventional minimum L1-norm approach. Source time-courses obtained from both simulated data and human MEG recordings show high temporal stability (continuity) with no loss of temporal resolution. These two features of VESTAL resulted from combining the essential spatial–temporal projection in Eq. (7) with the vector-based minimum L1-norm approach in Eq. (3). The vector-based approach is important because it ensures that the row-(spatial) space of matrix **D** accurately represents the reconstructed source maps so that no "ghost images" from other regions will be falsely created. Eq. (7) was based on the fact that the MEG sensor waveforms are linear functions of the source time-courses; no temporal constraints were introduced during the analysis. Although the linear relationship between MEG sensor signal and source amplitude is behind all MEG source estimation techniques, not all approaches ensure this linear relationship in a spatiotemporal sense as VESTAL does to the reconstructed source time-courses. Hence, method-specific "spiky-looking" artifacts that do not exist in the sensor waveforms may present in the source time-courses with some approaches (e.g., the conventional minimum L1-norm approaches in Matsuura and Okabe, 1995, 1997, 1999; Uutela et al., 1999, and commercial software packages like CURRY). A third strength of VESTAL is that it can resolve sources that are correlated 100%, as illustrated by the computer simulation, and also has no problem resolving uncorrelated sources. We consider this feature of VESTAL an improvement over many existing MEG and EEG localization methods including beamformer approaches, which assume that source time-courses are uncorrelated (Van Veen et al., 1997; Gross and Ioannides, 1999; Robinson and Vrba, 1999; Gross et al., 2001; Sekihara et al., 2001; Hillebrand and Barnes, 2003; Barnes and Hillebrand, 2003); and MUSIC, which assumes they are linearly independent (Mosher et al., 1992, 1999a; Mosher and Leahy, 1998).

We also examined the performance of VESTAL in obtaining information about source extent. Our computer simulation demonstrated that VESTAL can accurately obtain the source extent only if this information is not buried in noise, which generally requires very high SNR. With realistic SNR, VESTAL will provide focal images when no upper bound is imposed on the source strength. To obtain information about source extent under realistic SNR, additional information such as the maximum dipole moment density (dipole moment per mm^2) is needed to set a meaningful upper bound for the source strength. Such information can be obtained from invasive electro-neurophysiology studies in animals and humans. This issue regarding the source extent, however, applies to all inverse approaches.

The application of VESTAL to the median-nerve MEG response clearly demonstrated the great potential of this algorithm in distinguishing multiple sources in empirical human responses that are closely situated in space (e.g., BA 1, 2, 3b, 4, 5, and 7). The source location and latency results derived from VESTAL are highly consistent with the known neurophysiology of somatosensory system and previous studies (Rosen and Asanuma, 1972; Lemon and Porter, 1976; Jones et al., 1978; Wong et al., 1978; Jones et al., 1979; Lemon, 1979, 1981; Wood et al., 1985; Davidoff, 1990; Hari et al., 1993; Forss et al., 1994; Baldissera and Leocani, 1995; Kawamura et al., 1996; Mauguiere et al., 1997a,b; Jousmaki and Forss, 1998; Forss and Jousmaki, 1998; Hari and Forss, 1999; Spiegel et al., 1999; Boakye et al., 2000; Huang et al., 2000, 2004a, 2005; McGlone et al., 2002; Waberski et al., 2002).

The SII responses obtained from VESTAL in this example also agreed well with previous findings (Hari et al., 1993; Forss and Jousmaki, 1998; Hari and Forss, 1999; Fujiwara et al., 2002; Simoes et al., 2003; Huang et al., 2005). It was notable that an area in the ventral parietal cortex slightly posterior to SII was activated at about 110 ms, which is consistent with another report (Disbrow et al., 2001). The latencies of the sources obtained from VESTAL in the temporal lobe and temporal–parietal junction were later than that of the SII source, and very similar to another study (Tesche, 2000). Based on human and monkey studies, the temporal lobe source was believed to be at one of the unimodal association areas that subserved central vision, primary auditory, and somatosensory association areas, while the temporal–parietal junction source was a common area that was sensitive to multimodal sensory inputs (Jones and Powell, 1970; Seltzer and Pandya, 1978; Seltzer and Pandya, 1984; Baylis et al., 1987; Tesche, 2000). To our knowledge, this is the first case in which cortical areas in the somatosensory system have been mapped out *all at once* with high spatial resolution using MEG. In the temporal domain, the high stability and continuity of the source time-courses obtained by VESTAL demonstrate another major advantage of the algorithm.

In addition to the cortical areas, VESTAL showed early activation in the thalamus, which is consistent with several MEG and EEG studies (Tesche, 1996; Gobbele et al., 1998, 2004). Of course, more evidence is needed to confirm this thalamic activation, and to explore VESTAL's potential for localizing deep sources. Previous human MEG studies using electrical stimulation of finger and the median-nerve also reported activations in cerebellum (Tesche and Karhu, 1997, 2000). In the present example, we did not observe strong activation in the cerebellum. The discrepancy may be related to the different stimulation methods. Unlike our study, other paradigms (Tesche and Karhu, 1997, 2000) have included random omissions of 15% of the stimuli. This manipulation may produce attentional enhancement of the cerebella responses, possibly due to its role in fine-grained temporal tuning (Tesche and Karhu, 2000).

Acknowledgments

This work was supported in part by the Department of Radiology, University of California at San Diego, Merit Review Grants from the Department of Veterans Affairs (Huang, Lee, Harrington), and by National Institute of Health Grants R01-MH65304 (Canive), R21-MH067287 (Lewis), R01-EB00790 (Dale), R01-NS18741 (Halgren), R01-NS44623 (Halgren). We would also like to thank two anonymous reviewers' constructive suggestions that substantially strengthen the present study.

References

Aine, C., Huang, M., Stephen, J., Christner, R., 2000. Multistart algorithms for MEG empirical data analysis reliably characterize locations and time courses of multiple sources. NeuroImage 12, 159–172.

Auranen, T., Nummenmaa, A., Hamalainen, M.S., Jaaskelainen, I.P., Lampinen, J., Vehtari, A., Sams, M., 2005. Bayesian analysis of the neuromagnetic inverse problem with l(p)-norm priors. NeuroImage 26, 870–884.

Baldissera, F., Leocani, L., 1995. Afferent excitation of human motor cortex as revealed by enhancement of direct cortico-spinal actions on motoneurones. Electroencephalogr. Clin. Neurophysiol. 97, 394–401.

Barba, C., Frot, M., Guenot, M., Mauguiere, F., 2001. Stereotactic recordings of median nerve somatosensory-evoked potentials in the human pre-supplementary motor area. Eur. J. Neurosci. 13, 347–356.

Barnes, G.R., Hillebrand, A., 2003. Statistical flattening of MEG beamformer images. Hum. Brain Mapp. 18, 1–12.

Barros, A.K., Vigario, R., Jousmaki, V., Ohnishi, N., 2000. Extraction of event-related signals from multichannel bioelectrical measurements. IEEE Trans. Biomed. Eng 47, 583–588.

Baylis, G.C., Rolls, E.T., Leonard, C.M., 1987. Functional subdivisions of the temporal lobe neocortex. J. Neurosci. 7, 330–342.

Boakye, M., Huckins, S.C., Szeverenyi, N.M., Taskey, B.I., Hodge, C.J. Jr., 2000. Functional magnetic resonance imaging of somatosensory cortex activity produced by electrical stimulation of the median nerve or tactile stimulation of the index finger. J. Neurosurg. 93, 774–783.

Chvatal, V., 1983. Linear Programming. Freeman, New York.

Dale, A.M., Halgren, E., 2001. Spatiotemporal mapping of brain activity by integration of multiple imaging modalities. Curr. Opin. Neurobiol. 11, 202–208.

Dale, A.M., Fischl, B., Sereno, M.I., 1999. Cortical surface-based analysis: I. Segmentation and surface reconstruction. NeuroImage 9, 179–194.

Dale, A.M., Liu, A.K., Fischl, B.R., Buckner, R.L., Belliveau, J.W., Lewine, J.D., Halgren, E., 2000. Dynamic statistical parametric mapping: combining fMRI and MEG for high-resolution imaging of cortical activity. Neuron 26, 55–67.

Davidoff, R.A., 1990. The pyramidal tract. Neurology 40, 332–339.

Disbrow, E., Roberts, T., Poeppel, D., Krubitzer, L., 2001. Evidence for interhemispheric processing of inputs from the hands in human S2 and PV. J. Neurophysiol. 85, 2236–2244.

Eiselt, H.A., Pederzoli, G., Sandblom, C.-L., 1987. Continuous Optimization Models. Walter de Gruyter, Berlin.

Ferguson, A.S., Zhang, X., Stroink, G., 1994. A complete linear discretization for calculating the magnetic field using the boundary element method. IEEE Trans. Biomed. Eng. 41, 455–460.

Fischl, B., van der, K.A., Destrieux, C., Halgren, E., Segonne, F., Salat, D.H., Busa, E., Seidman, L.J., Goldstein, J., Kennedy, D., Caviness, V., Makris, N., Rosen, B., Dale, A.M., 2004. Automatically parcellating the human cerebral cortex. Cereb. Cortex 14, 11–22.

Forss, N., Jousmaki, V., 1998. Sensorimotor integration in human primary and secondary somatosensory cortices. Brain Res. 781, 259–267.

Forss, N., Hari, R., Salmelin, R., Ahonen, A., Hamalainen, M., Kajola, M., Knuutila, J., Simola, J., 1994. Activation of the human posterior parietal cortex by median nerve stimulation. Exp. Brain Res. 99, 309–315.

Fujiwara, N., Imai, M., Nagamine, T., Mima, T., Oga, T., Takeshita, K., Toma, K., Shibasaki, H., 2002. Second somatosensory area (SII) plays a significant role in selective somatosensory attention. Brain Res. Cogn. Brain Res. 14, 389–397.

Geman, S., Geman, D., 1984. Stochastic relaxation, gibbs distributions, and the Bayesian restoration of images. IEEE Trans. Pattern Anal. Mach. Intell. 6, 721–741.

Gobbele, R., Buchner, H., Curio, G., 1998. High-frequency (600 Hz) SEP activities originating in the subcortical and cortical human somatosensory system. Electroencephalogr. Clin. Neurophysiol. 108, 182–189.

Gobbele, R., Waberski, T.D., Simon, H., Peters, E., Klostermann, F., Curio, G., Buchner, H., 2004. Different origins of low- and high-frequency components (600 Hz) of human somatosensory evoked potentials. Clin. Neurophysiol. 115, 927–937.

Gorodnitsky, I.F., George, J.S., Rao, B.D., 1995. Neuromagnetic source imaging with FOCUSS: a recursive weighted minimum norm algorithm. Electroencephalogr. Clin. Neurophysiol. 95, 231–251.

Gross, J., Ioannides, A.A., 1999. Linear transformations of data space in MEG. Phys. Med. Biol. 44, 2081–2097.

Gross, J., Kujala, J., Hamalainen, M., Timmermann, L., Schnitzler, A., Salmelin, R., 2001. Dynamic imaging of coherent sources: studying neural interactions in the human brain. Proc. Natl. Acad. Sci. U. S. A. 98, 694–699.

Hamalainen, M.S., 2005. MNE Software User's Guide. NMR Center, Mass General Hospital, Harvard University.

Hamalainen, M.S., Ilmoniemi, R.J., 1994. Interpreting magnetic fields of the brain: minimum norm estimates. Med. Biol. Eng. Comput. 32, 35–42.

Hamalainen, M.S., Sarvas, J., 1989. Realistic conductivity geometry model of the human head for interpretation of neuromagnetic data. IEEE Trans. Biomed. Eng. 36, 165–171.

Hanlon, F.M., Weisend, M.P., Huang, M., Lee, R.R., Moses, S.N., Paulson, K.M., Thoma, R.J., Miller, G.A., Canive, J.M., 2003. A non-invasive method for observing hippocampal function. NeuroReport 14, 1957–1960.

Hari, R., Forss, N., 1999. Magnetoencephalography in the study of human somatosensory cortical processing. Philos. Trans. R. Soc. Lond., B Biol. Sci. 354, 1145–1154.

Hari, R., Karhu, J., Hamalainen, M., Knuutila, J., Salonen, O., Sams, M., Vilkman, V., 1993. Functional organization of the human first and second somatosensory cortices: a neuromagnetic study. Eur. J. Neurosci. 5, 724–734.

Hillebrand, A., Barnes, G.R., 2003. The use of anatomical constraints with MEG beamformers. NeuroImage 20, 2302–2313.

Huang, M., Aine, C.J., Supek, S., Best, E., Ranken, D., Flynn, E.R., 1998. Multi-start downhill simplex method for spatio-temporal source localization in magnetoencephalography. Electroencephalogr. Clin. Neurophysiol. 108, 32–44.

Huang, M.X., Aine, C., Davis, L., Butman, J., Christner, R., Weisend, M., Stephen, J., Meyer, J., Silveri, J., Herman, M., Lee, R.R., 2000. Sources on the anterior and posterior banks of the central sulcus identified from magnetic somatosensory evoked responses using multistart spatio-temporal localization. Hum. Brain Mapp. 11, 59–76.

Huang, M., Davis, L.E., Aine, C., Weisend, M., Harrington, D., Christner, R., Stephen, J., Edgar, J.C., Herman, M., Meyer, J., Paulson, K., Martin, K., Lee, R.R., 2004a. MEG response to median nerve stimulation correlates with recovery of sensory and motor function after stroke. Clin. Neurophysiol. 115, 820–833.

Huang, M.X., Harrington, D.L., Paulson, K.M., Weisend, M.P., Lee, R.R., 2004b. Temporal dynamics of ipsilateral and contralateral motor activity during voluntary finger movement. Hum. Brain Mapp. 23, 26–39.

Huang, M.X., Lee, R.R., Miller, G.A., Thoma, R.J., Hanlon, F.M., Paulson, K.M., Martin, K., Harrington, D.L., Weisend, M.P., Edgar, J.C., Canive, J.M., 2005. A parietal–frontal network studied by somatosensory oddball MEG responses, and its cross-modal consistency. NeuroImage 28, 99–114.

Ikeda, S., Toyama, K., 2000. Independent component analysis for noisy data-MEG data analysis. Neural Netw. 13, 1063–1074.

Ioannides, A.A., Singh, K.D., Hasson, R., Baumann, S.B., Rogers, R.L., Guinto, F.C. Jr., Papanicolaou, A.C., 1993. Comparison of single current dipole and magnetic field tomography analyses of the cortical response to auditory stimuli. Brain Topogr. 6, 27–34.

Jones, E.G., Powell, T.P., 1970. An anatomical study of converging sensory pathways within the cerebral cortex of the monkey. Brain 93, 793–820.

Jones, E.G., Coulter, J.D., Hendry, S.H., 1978. Intracortical connectivity of architectonic fields in the somatic sensory, motor and parietal cortex of monkeys. J. Comp. Neurol. 181, 291–347.

Jones, E.G., Wise, S.P., Coulter, J.D., 1979. Differential thalamic relationships of sensory-motor and parietal cortical fields in monkeys. J. Comp. Neurol. 183, 833–881.

Jousmaki, V., Forss, N., 1998. Effects of stimulus intensity on signals from human somatosensory cortices. NeuroReport 9, 3427–3431.

Jung, T.P., Makeig, S., Humphries, C., Lee, T.W., McKeown, M.J., Iragui, V., Sejnowski, T.J., 2000a. Removing electroencephalographic artifacts by blind source separation. Psychophysiology 37, 163–178.

Jung, T.P., Makeig, S., Westerfield, M., Townsend, J., Courchesne, E., Sejnowski, T.J., 2000b. Removal of eye activity artifacts from visual event-related potentials in normal and clinical subjects. Clin. Neurophysiol. 111, 1745–1758.

Jung, T.P., Makeig, S., Westerfield, M., Townsend, J., Courchesne, E., Sejnowski, T.J., 2001. Analysis and visualization of single-trial event-related potentials. Hum. Brain Mapp. 14, 166–185.

Kandel, E.R., Schwartz, J.H., Jessell, T.M., 2000. Principles of Neural Science. McGraw-Hill, New York.

Kawamura, T., Nakasato, N., Seki, K., Kanno, A., Fujita, S., Fujiwara, S., Yoshimoto, T., 1996. Neuromagnetic evidence of pre- and post-central cortical sources of somatosensory evoked responses. Electroencephalogr. Clin. Neurophysiol. 100, 44–50.

Lemon, R.N., 1979. Short-latency peripheral inputs to the motor cortex in conscious monkeys. Brain Res. 161, 150–155.

Lemon, R.N., 1981. Functional properties of monkey motor cortex neurones receiving afferent input from the hand and fingers. J. Physiol. 311, 497–519.

Lemon, R.N., Porter, R., 1976. Afferent input to movement-related precentral neurones in conscious monkeys. Proc. R. Soc. Lond., B Biol. Sci. 194, 313–339.

Liljestrom, M., Kujala, J., Jensen, O., Salmelin, R., 2005. Neuromagnetic localization of rhythmic activity in the human brain: a comparison of three methods. NeuroImage 25, 734–745.

Makeig, S., Jung, T.P., Bell, A.J., Ghahremani, D., Sejnowski, T.J., 1997. Blind separation of auditory event-related brain responses into independent components. Proc. Natl. Acad. Sci. U. S. A. 94, 10979–10984.

Marinkovic, K., Dhond, R.P., Dale, A.M., Glessner, M., Carr, V., Halgren, E., 2003. Spatiotemporal dynamics of modality-specific and supramodal word processing. Neuron 38, 487–497.

Matsuura, K., Okabe, Y., 1995. Selective minimum-norm solution of the biomagnetic inverse problem. IEEE Trans. Biomed. Eng. 42, 608–615.

Matsuura, K., Okabe, Y., 1997. A robust reconstruction of sparse biomagnetic sources. IEEE Trans. Biomed. Eng. 44, 720–726.

Matsuura, K., Okabe, Y., 1999. Multiple current-dipole distribution reconstruction reconstructed by modified selective minimum-norm method. In: Aine, C., Okada, Y.C., Stroink, G., Swithenby, S., Wood, C.C. (Eds.), Advances in Biomagnetism Research: Biomag96. Springer, New York, pp. 290–293.

Mauguiere, F., Merlet, I., Forss, N., Vanni, S., Jousmaki, V., Adeleine, P., Hari, R., 1997a. Activation of a distributed somatosensory cortical network in the human brain. A dipole modelling study of magnetic fields evoked by median nerve stimulation: Part I. Location and activation timing of SEF sources. Electroencephalogr. Clin. Neurophysiol. 104, 281–289.

Mauguiere, F., Merlet, I., Forss, N., Vanni, S., Jousmaki, V., Adeleine, P., Hari, R., 1997b. Activation of a distributed somatosensory cortical network in the human brain: a dipole modelling study of magnetic fields evoked by median nerve stimulation: Part II. Effects of stimulus rate, attention and stimulus detection. Electroencephalogr. Clin. Neurophysiol. 104, 290–295.

McGlone, F., Kelly, E.F., Trulsson, M., Francis, S.T., Westling, G., Bowtell, R., 2002. Functional neuroimaging studies of human somatosensory cortex. Behav. Brain Res. 135, 147–158.

Mosher, J.C., Leahy, R.M., 1998. Recursive MUSIC: a framework for EEG and MEG source localization. IEEE Trans. Biomed. Eng. 45, 1342–1354.

Mosher, J.C., Lewis, P.S., Leahy, R.M., 1992. Multiple dipole modeling and localization from spatio-temporal MEG data. IEEE Trans. Biomed. Eng. 39, 541–557.

Mosher, J.C., Baillet, S., Leahy, R.M., 1999. EEG source localization and imaging using multiple signal classification approaches. J. Clin. Neurophysiol. 16, 225–238.

Mosher, J.C., Leahy, R.M., Lewis, P.S., 1999. EEG and MEG: forward solutions for inverse methods. IEEE Trans. Biomed. Eng. 46, 245–259.

Osipova, D., Ahveninen, J., Jensen, O., Ylikoski, A., Pekkonen, E., 2005. Altered generation of spontaneous oscillations in Alzheimer's disease. NeuroImage 27, 835–841.

Phillips, J.W., Leahy, R.M., Mosher, J.C., 1997. MEG-based imaging of focal neuronal current sources. IEEE Trans. Med. Imag. 16, 338–348.

Pulvermuller, F., Shtyrov, Y., Ilmoniemi, R., 2003. Spatiotemporal dynamics of neural language processing: an MEG study using minimum-norm current estimates. NeuroImage 20, 1020–1025.

Robinson, S.E., Vrba, J., 1999. Functional neuroimaging by syntheticaperture magnetometry (SAM). In: Yoshimoto, T., Kotani, M., Kuriki, S., Karibe, H., Nakasato, N. (Eds.), Recent Advances in Biomagnetism. Tohoku Univ. Press, Sendai, Japan, pp. 302–305.

Rosen, I., Asanuma, H., 1972. Peripheral afferent inputs to the forelimb area of the monkey motor cortex: input–output relations. Exp. Brain Res. 14, 257–273.

Sano, A., 1993. Optimally regularized inverse of singular value decomposition and application to signal extrapolation. Signal Process. 30, 163–176.

Sarvas, J., 1987. Basic mathematical and electromagnetic concepts of the biomagnetic inverse problem. Phys. Med. Biol. 32, 11–22.

Schlitt, H.A., Heller, L., Aaron, R., Best, E., Ranken, D.M., 1995. Evaluation of boundary element methods for the EEG forward problem: effect of linear interpolation. IEEE Trans. Biomed. Eng. 42, 52–58.

Sekihara, K., Poeppel, D., Marantz, A., Koizumi, H., Miyashita, Y., 1997. Noise covariance incorporated MEG-MUSIC algorithm: a method for multiple-dipole estimation tolerant of the influence of background brain activity. IEEE Trans. Biomed. Eng. 44, 839–847.

Sekihara, K., Poeppel, D., Marantz, A., Koizumi, H., Miyashita, Y., 1999. MEG spatio-temporal analysis using a covariance matrix calculated from nonaveraged multiple-epoch data. IEEE Trans. Biomed. Eng. 46, 515–521.

Sekihara, K., Nagarajan, S.S., Poeppel, D., Marantz, A., Miyashita, Y., 2001. Reconstructing spatio-temporal activities of neural sources using an MEG vector beamformer technique. IEEE Trans. Biomed. Eng. 48, 760–771.

Seltzer, B., Pandya, D.N., 1978. Afferent cortical connections and architectonics of the superior temporal sulcus and surrounding cortex in the rhesus monkey. Brain Res. 149, 1–24.

Seltzer, B., Pandya, D.N., 1984. Further observations on parieto-temporal connections in the rhesus monkey. Exp. Brain Res. 55, 301–312.

Shih, J.J., Weisend, M.P., Davis, J.T., Huang, M., 2000. Magnetoencephalographic characterization of sleep spindles in humans. J. Clin. Neurophysiol. 17, 224–231.

Simoes, C., Jensen, O., Parkkonen, L., Hari, R., 2003. Phase locking between human primary and secondary somatosensory cortices. Proc. Natl. Acad. Sci. U. S. A. 100, 2691–2694.

Spiegel, J., Tintera, J., Gawehn, J., Stoeter, P., Treede, R.D., 1999. Functional MRI of human primary somatosensory and motor cortex during median nerve stimulation. Clin. Neurophysiol. 110, 47–52.

Stenbacka, L., Vanni, S., Uutela, K., Hari, R., 2002. Comparison of minimum current estimate and dipole modeling in the analysis of simulated activity in the human visual cortices. NeuroImage 16, 936–943.

Stephen, J.M., Aine, C.J., Christner, R.F., Ranken, D., Huang, M., Best, E., 2002. Central versus peripheral visual field stimulation results in timing differences in dorsal stream sources as measured with MEG. Vision Res. 42, 3059–3074.

Stephen, J.M., Davis, L.E., Aine, C.J., Ranken, D., Herman, M., Hudson, D., Huang, M., Poole, J., 2003. Investigation of the normal proximal somatomotor system using magnetoencephalography. Clin. Neurophysiol. 114, 1781–1792.

Tesche, C.D., 1996. Non-invasive imaging of neuronal population dynamics in human thalamus. Brain Res. 729, 253–258.

Tesche, C., 2000. Evidence for somatosensory evoked responses in human temporal lobe. NeuroReport 11, 2655–2658.

Tesche, C.D., Karhu, J., 1997. Somatosensory evoked magnetic fields arising from sources in the human cerebellum. Brain Res. 744, 23–31.

Tesche, C.D., Karhu, J.J., 2000. Anticipatory cerebellar responses during somatosensory omission in man. Hum. Brain Mapp. 9, 119–142.

Urbano, A., Babiloni, F., Babiloni, C., Ambrosini, A., Onorati, P., Rossini, P.M., 1997. Human short latency cortical responses to somatosensory stimulation. A high resolution EEG study. NeuroReport 8, 3239–3243.

Uutela, K., Hamalainen, M., Somersalo, E., 1999. Visualization of magnetoencephalographic data using minimum current estimates. NeuroImage 10, 173–180.

Vanni, S., Uutela, K., 2000. Foveal attention modulates responses to peripheral stimuli. J. Neurophysiol. 83, 2443–2452.

Van Veen, B.D., van, D.W., Yuchtman, M., Suzuki, A., 1997. Localization of brain electrical activity via linearly constrained minimum variance spatial filtering. IEEE Trans. Biomed. Eng. 44, 867–880.

Vigario, R.N., 1997. Extraction of ocular artefacts from EEG using independent component analysis. Electroencephalogr. Clin. Neurophysiol. 103, 395–404.

Vigario, R., Oja, E., 2000. Independence: a new criterion for the analysis of the electromagnetic fields in the global brain? Neural Netw. 13, 891–907.

Vigario, R., Sarela, J., Jousmaki, V., Hamalainen, M., Oja, E., 2000. Independent component approach to the analysis of EEG and MEG recordings. IEEE Trans. Biomed. Eng. 47, 589–593.

Waberski, T.D., Gobbele, R., Darvas, F., Schmitz, S., Buchner, H., 2002. Spatiotemporal imaging of electrical activity related to attention to somatosensory stimulation. NeuroImage 17, 1347–1357.

Wong, Y.C., Kwan, H.C., MacKay, W.A., Murphy, J.T., 1978. Spatial organization of precentral cortex in awake primates: I. Somatosensory inputs. J. Neurophysiol. 41, 1107–1119.

Wood, C.C., Cohen, D., Cuffin, B.N., Yarita, M., Allison, T., 1985. Electrical sources in human somatosensory cortex: identification by combined magnetic and potential recordings. Science 227, 1051–1053.